Neutral-strange-particle production in antiproton-proton reactions at 3.0 GeV/c

S. M. Jacobs, L. E. Kirsch, S. C. Moore, and P. E. Schmidt
Brandeis University, Waltham, Massachusetts 02154

T. Davis and B. T. Meadows
University of Cincinnati, Cincinnati, Ohio 45221

A. Fainberg, M. Goldberg, I. R. Linscott, G. C. Moneti, and D. P. Weygand
Syracuse University, Syracuse, New York 13210
(Received 26 September 1977)

The reactions $\bar{p}p \to V^0 +$ neutrals were studied in a multiparticle spectrometer at 3.0 GeV/c incident momentum, with a sensitivity of about 150 events/μb. Differential cross sections and polarization of the $\bar{\Lambda}$ for the final states $\bar{\Lambda}(\Lambda)$ and $\bar{\Lambda}(\Sigma^0)$ are reported and compared with theoretical models. Differential cross sections of the K^0 in K^0 [$K^*(890)$] and the Λ in $\Lambda(\bar{\Lambda} + \bar{\Sigma}^0)$ are also measured. Upper limits of a few μb MeV are obtained for the formation of narrow resonances decaying into $V^0 +$ neutrals in the mass interval 2.74–2.80 GeV/c^2.

I. INTRODUCTION

We present a measurement of the reactions

$$\bar{p}p \to \bar{\Lambda}^0 + \text{neutrals}, \quad (1)$$

$$\to \Lambda^0 + \text{neutrals}, \quad (2)$$

$$\to K_S^0 + \text{neutrals} \quad (3)$$

in the forward hemisphere of the center of mass at 3.0 GeV/c incident laboratory momentum. The data were obtained at the Brookhaven National Laboratory (BNL) multiparticle spectrometer (MPS)[1] using the medium-energy separated beam (MESB) and correspond to an observed sensitivity of ~ 150 events/μb.

Reaction (1) at this energy is dominated by two-body final states such as

$$\bar{p}p \to \bar{\Lambda}\Lambda, \quad (4)$$

$$\to \bar{\Lambda}\Sigma^0 + \bar{\Sigma}^0\Lambda, \quad (5)$$

whose differential cross section and polarization provide tests of Regge models of hypercharge-exchange processes.[2,3] These final states have been studied with smaller statistics in bubble-chamber experiments.[4] Reaction (2) is forbidden by the usual exchange processes but could proceed via s-channel interactions, or $B=2$, $S=1$ particle exchanges.

Reaction (3) allows us to study the isovector hyperon exchange for two-body processes such as

$$\bar{p}p \to \bar{K}^0 K^0, \quad (6)$$

$$\to \bar{K}^0 K^{*0}(890). \quad (7)$$

Since the center-of-mass energy is in the region of 2.8 GeV, the data can be used to search for the formation of narrow-width states such as the η_c, the lowest pseudoscalar member of the charmonium system.

The experimental procedure is described in Sec. II, and the data analysis and the results on differential cross sections and polarization are presented in Sec. III. In Sec. IV we report on our search for narrow states in formation. Our data on hypercharge-exchange reactions are compared with previous experiments and some models in Sec. V. Finally, the conclusions are presented in Sec. VI.

II. EXPERIMENTAL PROCEDURE

A. Experimental setup

The MPS configuration of the target region for this experiment is shown in Fig. 1, and a complete description of this detector is given in Ref. 1. The MESB was tuned to select antiprotons with its

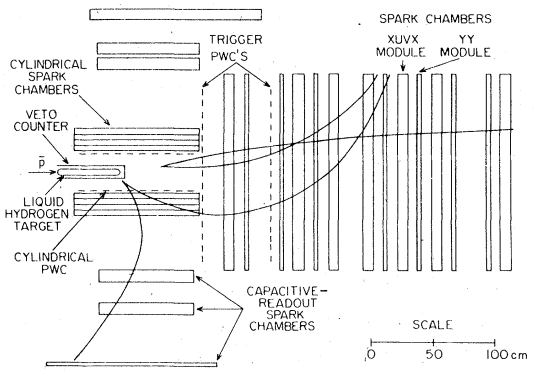

FIG. 1. Target region of the MPS.

maximum momentum acceptance of ± 3%. A beam spectrometer consisting of six proportional wire chambers (PWC's) measured the momentum of each particle to approximately 0.5%, and the incident angles to 0.4 mrad at the entrance to the target vacuum jacket. The beam of $\sim 2.5\times 10^4$ antiprotons/pulse was identified by a threshold Čerenkov counter, with negligible K^- and $\sim 0.5\%$ π^- contamination. A 50-cm-long, 7.6-cm-diameter liquid hydrogen target was surrounded by a 0.64-cm-thick veto counter consisting of two semicylinders of 5.7-cm radius and a planar downstream endcap. The target was further surrounded by a cylindrical PWC, a set of five cylindrical spark chambers, and ten planar capacitive-readout spark chambers on each side.

About 60 cm downstream of the veto counter were two planes of PWC's ($TPX1, TPX2$) which were used to form the trigger:

$$(\bar{p}\,\text{beam})\cdot(\text{target veto})\cdot(2\text{–}3\ \text{tracks in}\ TPX1\cdot TPX2).$$

The MPS magnet was operated at 5 kG with the principal field component along the vertical (y) axis. The downstream tracks produced by the decay of the neutral V^0 were measured in 14 modules of magnetostrictive-readout spark chambers, half of which contained $xuvx$ gaps and half yy gaps.[1] Typically, 5% of the triggers were eventually reconstructed and identified as belonging to reactions 1–3.

The decay products of a neutral V^0 produced at large angles were measured in the cylindrical and capacitive spark chambers. The data presented in this paper are based on the downstream V^0's only.

B. Data analysis

The spark position measured in the magnetostrictive-readout chambers was corrected for ion drifts in the magnetic field by using beam tracks which are measured by the beam spectrometer outside of the MPS field volume, and then projected through the magnet. The difference between the projected and actual spark positions provided a correction for each plane. The data were first processed through a pattern recognition program which assembled the sparks into tracks, and then by a geometry program which calculated the trajectory of a particle through the varying magnetic field and minimized deviations from measured spark positions as a function of track parameters. The parameters for each pair of oppositely charged tracks were extrapolated through the magnetic field to determine the point of closest approach. The pair with minimum spatial separation was retained. A neutral track was defined by the sum of the charged-particle momenta at this vertex. Its intersection point with the incident particle measured in the beam spectrometer determined the V^0 production vertex.

The following selection criteria were then applied to all the data:

(1) The V^0 production vertex was required to be

TABLE I. Efficiency factors for total cross sections for typical two-body final states.

	Observed V^0 (missing neutrals)		
	$\bar{\Lambda}^0(\Lambda^0)$	$K^0[K^*(890)]$	$\Lambda^0(\bar{\Lambda}^0+\Sigma^0)$
Acceptance (%)			
Trigger efficiency [a]	4.9 ± 0.3	1.3 ± 0.1	3.9 ± 0.2
Spark-chamber and software efficiency [b]	65 ± 7	69 ± 8	41 ± 5
Selections [c] (%)			
e^+e^- pair rejection	99.2	93.3	92.9
V^0 mass and missing mass	74.5	68.6	78.5
V^0 opening angle	97.6	100.0	100.0
Target and veto	90.5	91.5	90.2
Lifetime	99.0	98.8	97.7
Minimum track length	88.0	92.8	•••
Production angle [d]	78.6	•••	•••
Total (%)	1.42 ± 0.21	0.49 ± 0.07	1.03 ± 0.16

[a] This factor includes geometrical acceptance as well as all trigger device efficiencies.
[b] The spark chamber and software efficiencies account for the loss of tracks with an insufficient number of chambers for event reconstruction.
[c] The selections are made in the order listed. The corresponding percentages are not cumulative.
[d] The production-angle selection was used only in the total cross-section determination (see text).

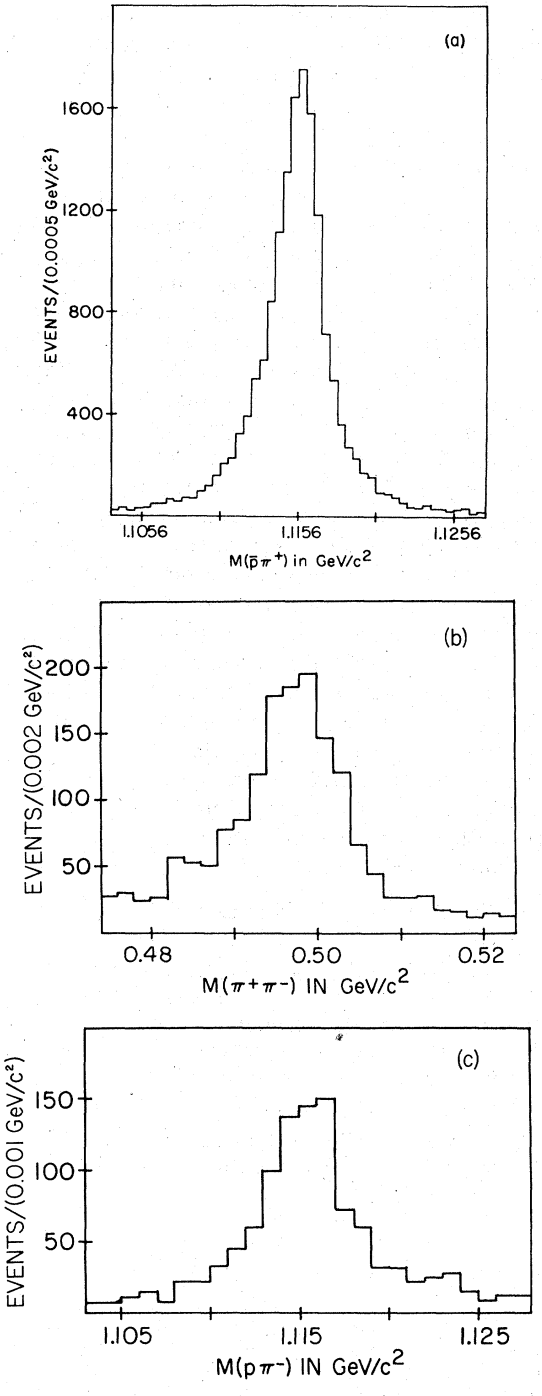

FIG. 2. Effective-mass spectrum and total number of events after selections for (a) $\bar{p}\pi^+$ (15712), (b) $\pi^+\pi^-$ (1642), (c) $p\pi^-$ (1077).

within the target volume and the V^0 decay vertex to be outside of the target veto counter.

(2) The lifetime of the V^0 was less than five times the standard value for the hypothesized particle.

(3) The effective mass of the V^0 when considered as an e^+e^- pair was greater than 40 MeV/c^2.

(4) The V^0 opening angle was greater than 3.7°.

(5) The computed exit point of both tracks from the MPS was at least 150 cm downstream from the target.

The effect of each of these criteria for some representative two-body final states is given in Table I.

Since the peripheral production of $\bar{\Lambda}^0$'s is an order of magnitude greater than the other processes, we first selected candidates for this reaction from the effective mass spectrum shown in Fig. 2(a).

The peak has a full width at half maximum of 3.0 MeV/c^2. A total of 13450 events with 1111.6 $< m_{\bar{p}\pi^+} <$ 1119.6 MeV/c^2 are considered to be $\bar{\Lambda}^0$'s. The background which is estimated to be less than 3% could either be Λ^0's, K_S^0's, e^+e^- pairs, or interactions which are recorded due to the target-veto inefficiency.

The K^0 and Λ^0 candidates initially contain more background. Thus more stringent selection criteria than given above were applied to these data.

To be considered as a K_S^0, we required that the V^0 mass was not that of a $\bar{\Lambda}^0$, Λ^0 or electron pair:

$$m_{\bar{p}\pi^+} < 1102 \text{ MeV}/c^2 \text{ or } m_{\bar{p}\pi^+} > 1130 \text{ MeV}/c^2,$$

$$m_{p\pi^-} < 1108 \text{ MeV}/c^2 \text{ or } m_{p\pi^-} > 1122 \text{ MeV}/c^2,$$

$$m_{e^+e^-} > 280 \text{ MeV}/c^2.$$

The effective mass of the remaining events is shown in Fig. 2(b). A total of 1170 events with $488 < m_{\pi^+\pi^-} < 506$ MeV/c^2 constitute the sample of K^0's, with a background of 16.5%.

To be considered as a Λ^0, we required that the V^0 mass was not that of a K^0 or electron pair:

$$m_{\pi^+\pi^-} < 490 \text{ MeV}/c^2 \text{ or } m_{\pi^+\pi^-} > 506 \text{ MeV}/c^2,$$

$$m_{e^+e^-} > 100 \text{ MeV}/c^2.$$

In addition, criterion (5) was not imposed. The effective mass of the remaining events is shown in Fig. 2(c). A total of 866 events with 1110 $< m_{p\pi^-} <$ 1121 MeV/c^2 constitute the sample of Λ^0's, with a background of 11%.

To investigate the effect of the contamination in the K^0 and Λ^0 samples, we have examined the distribution of missing mass and four-momentum transfer squared to the V^0 in control regions just outside the K^0 and Λ^0 combined mass peaks, and compared them to the corresponding distributions for our selected K^0 and Λ^0 samples. Except for two-body production these distributions have quite similar characteristics. Thus we expect negligible

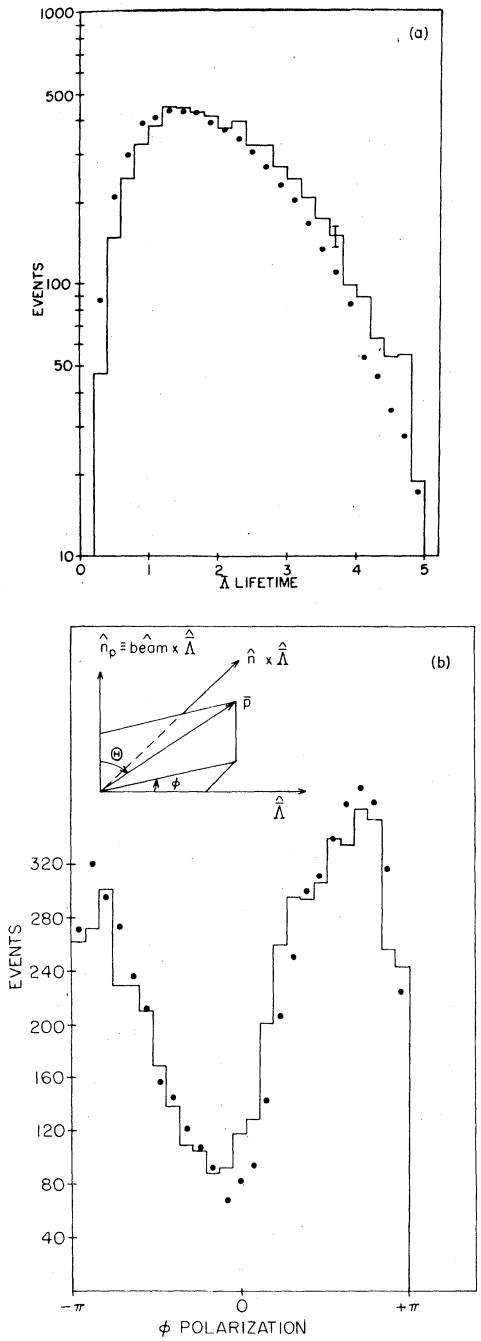

FIG. 3. (a) Comparison of observed and predicted $\bar{\Lambda}^0$ lifetime distribution in units of $c\tau$=7.73 cm. (b) Comparison of observed and predicted $\phi_{\text{polarization}}$ in units of radians.

bias from this contamination.

In order to improve the missing-mass resolution, a one-constraint kinematic fit was applied to the V^0's using the hypothesized mass. The point of intersection between the neutral track and the beam was then corrected using the new V^0 direction.

C. Acceptance

A Monte Carlo program was used to simulate reactions in the MPS. Identical selection criteria were applied to the Monte Carlo events and the data. In addition, we attempted to simulate losses of events due to hardware efficiency, pattern recognition requirements, and measurement resolution. As a test of our understanding we have selected, from the missing-mass distribution, the subset of reaction (1) which belongs to the final state $\bar{p}p \to \bar{\Lambda}^0(\Lambda^0)$. An extensive comparison of experimental and Monte Carlo distributions was then performed in order to ensure that all effects had been properly accounted for. As an example, we show in Fig. 3(a) the lifetime distribution of the $\bar{\Lambda}^0$ for both Monte Carlo and data. In Fig. 3(b) we show the azimuthal angular distribution of the decay antiproton in the $\bar{\Lambda}^0$ center of mass with respect to the normal to the production plane $\hat{n}$. Although both Monte Carlo distributions display some systematic deviations from the data, the general shape is reproduced.

III. EXPERIMENTAL RESULTS

A. $\bar{\Lambda}^0$ production

1. Missing-mass spectrum

The distribution of the square of the missing mass m_X^2 recoiling against the $\bar{\Lambda}^0$ is shown in Fig. 4. The spectrum is dominated by the two-body states $\bar{\Lambda}^0\Lambda^0$, $\bar{\Lambda}^0\Sigma^0+\bar{\Sigma}^0\Lambda^0$ and includes a signal for $\bar{\Lambda}^0\Lambda^0(1520)$. There is no obvious evidence for $\bar{\Lambda}^0\Sigma^0(1385)$ or $\bar{\Lambda}^0\Lambda^0(1405)$. In order to isolate the $\bar{\Lambda}\Lambda$ and $\bar{\Lambda}\Sigma^0$ events, we selected m_X^2 < 1.6 $(\text{GeV}/c^2)^2$ and performed a fit for the fractions of the following contributions:

(a) a Gaussian shape for the Λ^0 and Σ^0,

(b) a calculated $\Lambda^0\gamma$ effective mass spectrum from the final state $\bar{\Sigma}^0\Lambda^0$ followed by $\bar{\Sigma}^0 \to \bar{\Lambda}^0\gamma$

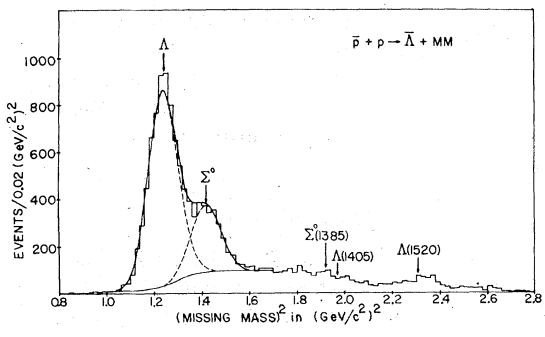

FIG. 4. Missing-mass spectrum for $\bar{p}p \to \bar{\Lambda}^0 X$. Total events: 13414.

decay, with approximate resolution folded in, and
(c) a quadratic background.

We assumed equal missing-mass resolutions for Λ^0 and Σ^0, and identical production rates for $\bar{\Lambda}^0\Sigma^0$ and $\bar{\Sigma}^0\Lambda^0$. From the fit, the number of $\bar{\Lambda}\Lambda$ and $\bar{\Lambda}\Sigma^0$ events in the m_X^2 spectrum was determined to be 5789 and 1625, respectively.

Since the falling edge of the spectrum described in (b) is near the $\Sigma^0(1385)$ and the missing-mass resolution in this region prevents the separation of the $\Sigma^0(1385)$ from the $\Lambda(1405)$, we are unable to cleanly resolve these states or to quote a cross section for them.

In order to select the $\bar{\Lambda}\Lambda$ and $\bar{\Lambda}\Sigma^0$ event sample, we then required $1.155 < m_X^2 < 1.315$ $(\mathrm{GeV}/c^2)^2$ for the Λ^0 and $1.335 < m_X^2 < 1.495$ $(\mathrm{GeV}/c^2)^2$ for the Σ^0. This results in a $\bar{\Lambda}\Lambda$ $(\bar{\Lambda}\Sigma^0)$ data sample which contains 84% (84%) of the events from the above fit, with a background of 5% (33%). The large background under the Σ^0 is mostly due to the charge-conjugate $\bar{\Sigma}^0\Lambda$ events, which have approximately the same angular distribution as the $\bar{\Lambda}\Sigma^0$ events.

Since the fraction of the missing-mass spectrum belonging to the two-body final states varies as a function of $\bar{\Lambda}^0$ production angle, the χ^2 fit described above was repeated in several momentum-transfer intervals. This yields the production angular distribution, which was then corrected for acceptance using the Monte Carlo calculation. Because of the non-Gaussian tails in the effective- and missing-mass distributions, the loss of events due to the cuts in these spectra was determined directly from the data.

2. *Total cross sections*

The total cross sections for these final states were measured using the subset of events in the production angular region $0.85 < \cos\theta^* < 1.00$. The resulting partial cross sections for this region were then extrapolated over the entire forward hemisphere where the shape of the differential cross sections had been corrected for acceptance. The total cross sections are given in Table II. The cross section for the $\bar{\Lambda}\Lambda(1520)$ state was determined in a similar fashion using a subset of the data where $-t' < 0.1$ $(\mathrm{GeV}/c)^2$ and is contained in Table II. A summary of the momentum dependence of this cross section is given by Atherton *et al.*[4]

3. *Differential cross sections*

The production angular distributions were normalized in the restricted angular region described above to determine the differential cross sections. The data are recorded as a function of $t' = t - t_{\min}$ in Table III and displayed in Figs. 5(a) and 5(b). The errors are statistical and do not reflect the overall uncertainty in the total cross section of 15%.

TABLE II. Total cross sections. σ_{tot} is defined as the cross section in the forward hemisphere in the center of mass. The values are for observed final states and do not include the charge-conjugate reaction. The cross sections are corrected for decay branching ratios and backgrounds in the missing-mass spectra.

Final state	Acceptance (%)	σ_{tot} (μb)
$\bar{\Lambda}\Lambda$	1.42 ± 0.21	91 ± 14
$\bar{\Lambda}\Sigma^0$	1.09 ± 0.16	34 ± 6
$\bar{\Lambda}\Lambda(1520)$	0.27 ± 0.04	15.2 ± 3.3
$K^0K^*(890)$	0.49 ± 0.07	2.0 ± 0.4
K^0X $(M_X^2 > 1.0)$	0.32 ± 0.05	74 ± 11
K^0K^0 (upper limit)	1.64 ± 0.25	< 0.50
$\Lambda(\bar{\Lambda} + \bar{\Sigma}^0)$	1.03 ± 0.16	2.6 ± 0.5
ΛX $(M_X^2 > 1.5)$	0.77 ± 0.12	11.7 ± 1.9

The distributions show a distinct change to a flatter slope near $-t' \sim 0.35$ $(\mathrm{GeV}/c)^2$. The results of a fit to a functional form used by Atherton *et al.*,[4]

$$\begin{aligned} &a\exp(bt'), \quad -t' < -t'_B \\ &a\exp(bt'_B)\exp[c(t'-t_B)], \quad -t' > -t'_B \end{aligned} \tag{8}$$

TABLE III. Differential cross sections and polarization for $\bar{\Lambda}\Lambda^0$ and $\bar{\Lambda}\Sigma^0$ final states.

	Differential cross section $[\mu\mathrm{b}/(\mathrm{GeV}/c)^2]$	
$-t'$ $(\mathrm{GeV}/c)^2$	$\bar{\Lambda}\Lambda$	$\bar{\Lambda}\Sigma^0$
0.00–0.04	589.6 ± 15.8	200.5 ± 7.7
0.04–0.08	427.5 ± 13.8	130.5 ± 6.3
0.08–0.12	301.9 ± 12.1	98.1 ± 5.5
0.12–0.16	206.4 ± 10.0	68.3 ± 4.6
0.16–0.20	128.6 ± 7.7	54.8 ± 4.2
0.20–0.28	98.7 ± 5.3	33.1 ± 2.2
0.28–0.36	55.8 ± 4.2	18.1 ± 1.7
0.36–0.44	27.9 ± 3.0	14.2 ± 1.6
0.44–0.56	23.5 ± 2.6	12.2 ± 1.3
0.56–0.68	15.0 ± 2.3	7.7 ± 1.2
0.68–0.80	10.4 ± 2.3	8.9 ± 1.6
0.80–0.96	11.1 ± 2.5	9.1 ± 1.7
0.96–1.20	5.3 ± 1.7	3.0 ± 0.9
	Polarization	
$-t'$ $[(\mathrm{GeV}/c)^2]$	$\bar{\Lambda}\Lambda$	$\bar{\Lambda}\Sigma^0$
0.00–0.04	0.10 ± 0.07	0.14 ± 0.10
0.04–0.08	0.24 ± 0.08	0.25 ± 0.12
0.08–0.12	0.11 ± 0.10	0.69 ± 0.13
0.12–0.16	0.29 ± 0.12	0.36 ± 0.18
0.16–0.20	0.24 ± 0.16	0.16 ± 0.21
0.20–0.28	-0.28 ± 0.14	0.11 ± 0.18
0.28–0.44	-0.15 ± 0.16	0.02 ± 0.20
0.44–1.20	-0.27 ± 0.20	0.01 ± 0.19

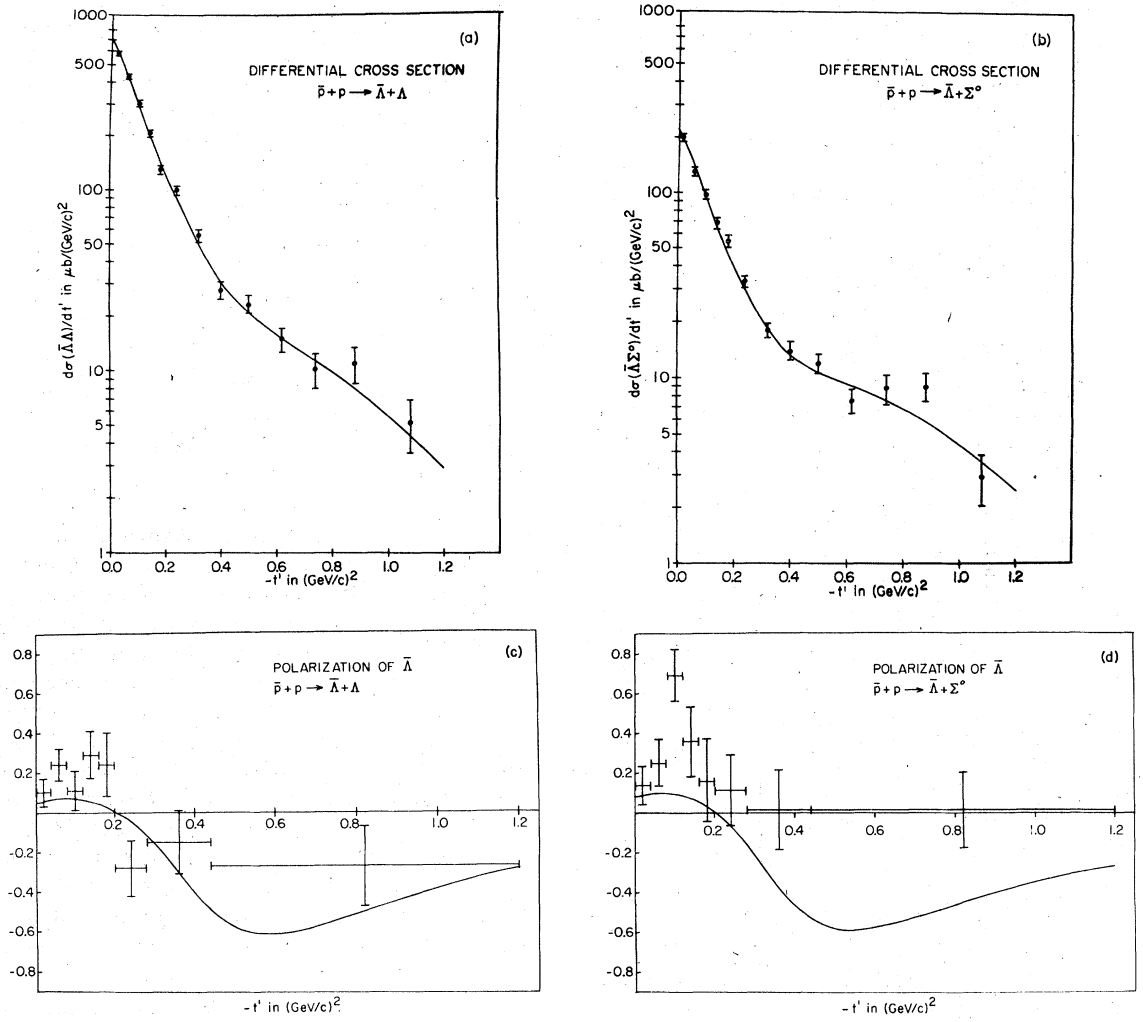

FIG. 5. Differential cross section $d\sigma/dt'$ for (a) $\bar{p}p \rightarrow \bar{\Lambda}^0\Lambda^0$, (b) $\bar{p}p \rightarrow \bar{\Lambda}^0\Sigma^0$. Polarization for (c) $\bar{p}p \rightarrow \bar{\Lambda}^0\Lambda^0$, (d) $\bar{p}p \rightarrow \bar{\Lambda}^0\Sigma^0$. The number of events of $\bar{\Lambda}^0\Lambda^0$ and $\bar{\Lambda}^0\Sigma^0$ are 5707 and 2747, respectively. The curves are the result of fits to the differential cross section using the Regge model of Plaut. The fitted parameters are given in Table IV.

with a, b, c, and t_B as free parameters, is given in Table IV. Also given are the results of a fit to a physically more attractive parametrization:

$$a \exp(bt') + c \exp(dt') . \tag{9}$$

4. Polarization

The polarization in each t' interval was determined by performing a fit to a straight line in the variable $(\hat{n} \cdot \hat{p}_{\bar{p}})_{\bar{\Lambda}\text{c.m.}}$, where $\hat{n}$ is the normal to the production plane, and demanding an acceptable value of χ^2. In a total of 200 bins in 16 angular distributions of the above variable only one bin was rejected as being statistically unlikely. The total χ^2 probability was 19%. As an additional check, we have measured the polarization at large $-t'$ for three different regions of the azimuthal polarization angle ϕ [Fig. 3(b)]. They all agree within errors. The t' dependence of the polarization for $\bar{\Lambda}\Lambda$ and $\bar{\Lambda}\Sigma^0$ final states is shown in Figs. 5(c) and 5(d). For the $\bar{\Lambda}\Lambda$ events, the polarization changes sign at $-t' \sim 0.25$ $(GeV/c)^2$ which is approximately the same value of momentum transfer where the differential cross section changes to a flatter slope. This effect is less clear for the $\bar{\Lambda}\Sigma$ data.

B. K^0 production

In Fig. 6 we show the missing-mass spectrum from reaction (3). There is clear evidence for $K^0_S K^{*0}(890)$ production and perhaps a small amount of $K^0_S K^0$. The cross section for the former and an upper limit for the latter are given in Table II.

TABLE IV. Parameters obtained from fits to the differential cross section. See text for parameter definition. The error in total cross section is not included in the parameter errors.

Reaction	Form of differential cross section Two exponentials [Eq. (8)]	Parameters a [μb/(GeV/c)^2]	b [(GeV/c)$^{-2}$]	c [(GeV/c)$^{-2}$]	$-t_B$ [(GeV/c)^2]	χ^2 probability
$\bar{p}p \to \bar{\Lambda}\Lambda$		689 ± 17	8.41 ± 0.20	2.41 ± 0.41	0.38 ± 0.02	0.04
$\to \bar{\Lambda}\Sigma^0$		225 ± 8	8.16 ± 0.31	1.88 ± 0.31	0.32 ± 0.02	0.19
$\pi^- p \to \Lambda^0 K^{0\,a}$		386 ± 34	8.6 ± 0.6	1.8 ± 0.2	0.34 ± 0.03	
	Sum of exponentials [Eq. (9)]	a [μb/(GeV/c)^2]	b [(GeV/c)$^{-2}$]	c [μb/(GeV/c)^2]	d [(GeV/c)$^{-2}$]	
$\bar{p}p \to \bar{\Lambda}\Lambda$		684 ± 19	9.66 ± 0.47	34 ± 14	1.58 ± 0.55	0.12
$\to \bar{\Lambda}\Sigma^0$		220 ± 9	10.32 ± 0.73	19 ± 6	1.38 ± 0.41	0.11
	Regge model	β_{+-} (GeV^{-1})	β_{++}	E_R (GeV^{-2})	λ_0	
$\bar{p}p \to \bar{\Lambda}\Lambda$		−2.00 ± 0.67	5.13 ± 0.07	1.77 ± 0.30	0.75 ± 0.03	0.16
$\to \bar{\Lambda}\Sigma^{0\,b}$		−1.34 ± 0.40	4.17 ± 0.07	1.39 ± 0.26	0.86 ± 0.03	0.25

[a] Reference 12.
[b] The parameters β_{++} and β_{+-} for this reaction represent, according to factorization, the expressions $\beta_{++} = [\beta_{++}(\bar{\Lambda})\beta_{++}(\Sigma^0)]^{1/2}$ and $\beta_{+-} = [\beta_{+-}(\bar{\Lambda})\beta_{+-}(\Sigma^0)]^{1/2}$.

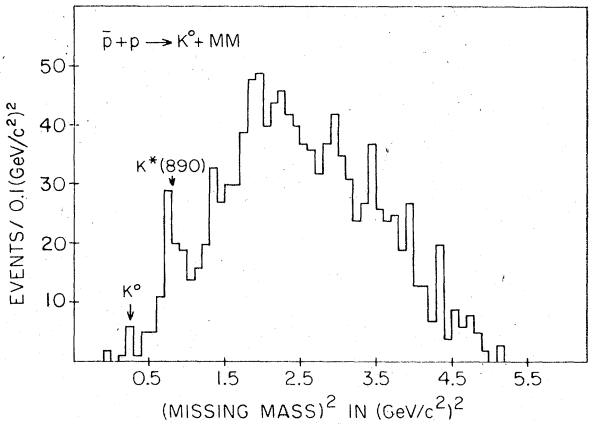

FIG. 6. Missing-mass spectrum for $\bar{p}p \to K_S^0 X$. Total events: 1170.

No other two-body states are observed. In order to estimate the contribution of multiparticle final states, we assumed a phase-space distribution for the momenta with a production angular dependence for the observed K_S^0 which matches the data. The missing-mass distribution was then corrected for acceptance of the observed particle. The experimental spectrum, after subtraction of the two-body states, is consistent with $K_S^0 K^0 \pi^0 \pi^0$ production with or without intermediate $K^*(890)$ states. Using the same technique, the final state $K_S^0 K^0 \pi^0$ would result in a sharp rise in this distribution near threshold at 0.4 (GeV/c^2)^2. Such a rise is not observed, which implies that there is no substantial contribution from this state. A cross

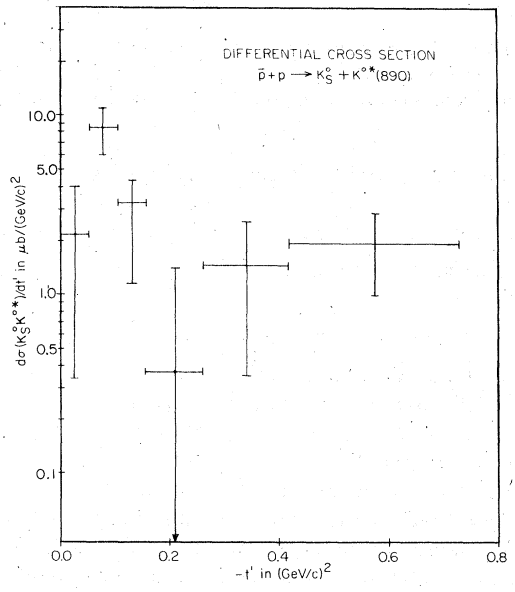

FIG. 7. Differential cross section $d\sigma/dt'$ for $\bar{p}p \to K_S^0 K^*(890)$. Total events: 79.

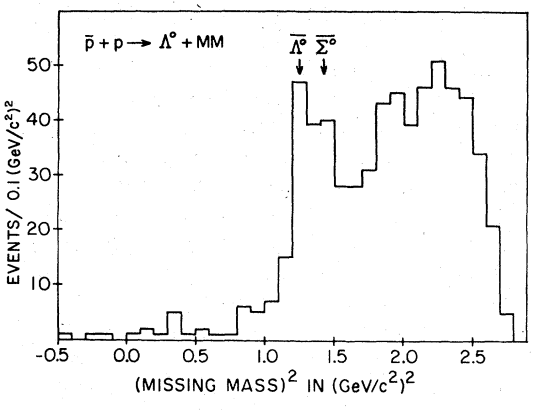

FIG. 8. Missing-mass spectrum for $\bar{p}p \rightarrow \Lambda^0 X$ in the forward hemisphere in the center of mass. Total events: 637.

section for these inclusive data was obtained assuming the final state $K^0K^{*0}(890)\pi^0$ and is contained in Table II.

The $K^0K^*(890)$ events were selected by the criterion $0.6 < m_X^2 < 1.0$ $(\mathrm{GeV}/c^2)^2$, which results in a background of approximately 55%. In Fig. 7 we present the differential cross section for this final state corrected for acceptance, and with background subtracted.

C. Λ^0 production

In Fig. 8 we show the missing-mass spectrum for reaction (2) with the selection of events in the forward hemisphere. The only structure corresponds to the two-body reactions $\Lambda\bar{\Lambda}$ and $\Lambda\bar{\Sigma}^0$. The remainder of the spectrum is consistent with three- and four-body final states $\Lambda\bar{\Lambda}\pi^0$ and $\Lambda\bar{\Lambda}\pi^0\pi^0$ as well as $\Sigma^0\bar{\Lambda}$. A cross section for these inclusive data was obtained assuming the final state $\Lambda^0\bar{\Lambda}^0\pi^0$ and is contained in Table II.

Owing to the limited data we have treated the $\bar{\Lambda}$ and $\bar{\Sigma}^0$ events together using the selection criterion $1.0 < m_X^2 < 1.5$ $(\mathrm{GeV}/c^2)^2$, which results in a background of $\sim 36\%$. The total cross section for this reaction is given in Table II.

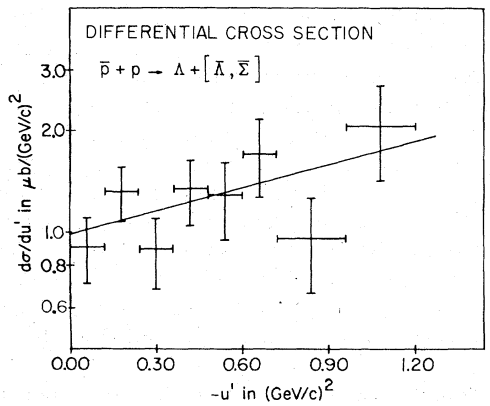

FIG. 9. Differential cross section $d\sigma/du'$ for $\bar{p}p \rightarrow \Lambda^0(\bar{\Lambda}^0 + \bar{\Sigma}^0)$. Total events: 148.

The differential cross section for these events is shown in Fig. 9. The data are consistent with a parametrization of the form $d\sigma/du' = ae^{bu'}$ with $a = 0.98 \pm 0.15$ μb/(GeV/c)^2 and $b = -0.52 \pm 0.29$ (GeV/c)$^{-2}$. The Λ^0 polarization was measured in the range $0.0 < -u' < 1.2$ $(\mathrm{GeV}/c)^2$ to be $P = 0.50 \pm 0.21$. This is the first measurement of the forward production of Λ's in an antiproton beam.

IV. SEARCH FOR NARROW STATES IN FORMATION

Soon after the discovery of the J/ψ it was hypothesized[5] that there should exist a $^1S_0$ bound state of the $c\bar{c}$ system, the η_c, in the mass region 3000–3100 MeV/c^2. An experiment performed at that time to search for the formation of the η_C in the reaction

$$\bar{p}p \rightarrow \eta_c \rightarrow V^0 + \text{neutrals}$$

did not observe any signal.[6]

In the interim, a DASP group[7] reported a peak with a mass of 2750± 100 MeV/c^2 in the reaction

$$e^+e^- \rightarrow \psi \rightarrow \eta_c\gamma \searrow \gamma\gamma .$$

No hadronic modes of this state have been reported, and the SLAC-LBL collaboration has set an upper limit[8] on the branching ratios $B(\psi \rightarrow \gamma\eta_c) \times B(\eta_c \rightarrow \bar{p}p)$ of 4×10^{-5}. The most recent value for the mass of the state found by the DASP group is 2830± 30 MeV/c^2.[9]

We have carried out a search for the formation of narrow states such as the η_C in the mass interval $2740 < M < 2800$ MeV/c^2, which is available to this experiment.

The measurement of the momentum of individual antiprotons in the beam spectrometer allows us to determine the center-of-mass energy of each event to ± 4.9 MeV, while the large momentum aperture of the beam spans the energy range. Since a spin-zero state decays isotropically, we can suppress the background and gain sensitivity by examining inclusive reactions such as forward production of Λ^0 and K^0, which are suppressed by the usual dynamical processes. Moreover, an elementary SU(3) calculation[10] suggests that the coupling of η_c to $\bar{p}p$ is approximately equal to the coupling to $\bar{\Lambda}\Lambda$.

Rather than measuring the flux and calculating the acceptance at each energy, we can use the fact that the center-of-mass energy dependence of the cross section for the peripherally produced events is not expected to display any structure.

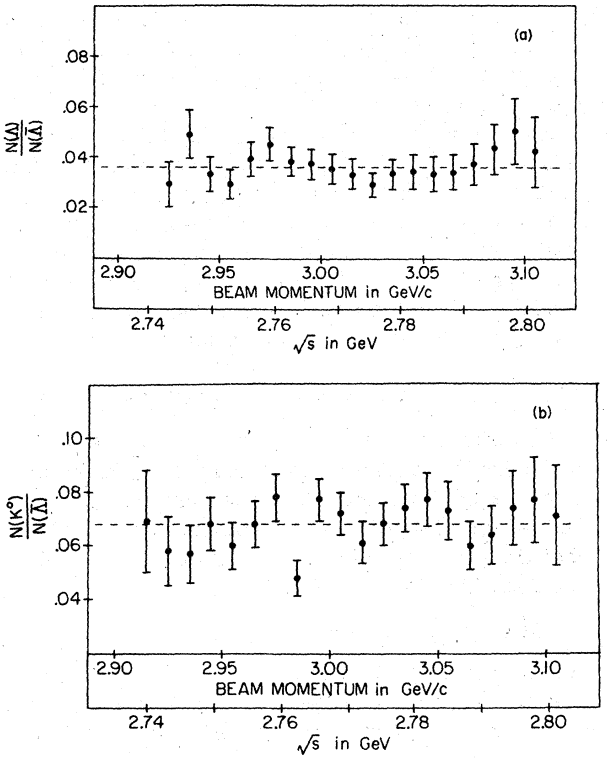

FIG. 10. (a) Number of forward Λ^0 events/No. of forward $\bar{\Lambda}^0$ events as a function of total center-of-mass energy. (b) Number of forward K^0 events/No. of forward $\bar{\Lambda}^0$ events as a function of total center-of-mass energy.

Then the ratios

$$R_1 = \text{No.}\Lambda/\text{No.}\bar{\Lambda}\ ,\quad R_2 = \text{No.}K^0/\text{No.}\bar{\Lambda}$$

will directly be sensitive to the formation of any resonant states. The data are shown in Fig. 10, and indicate no anomalous behavior. Using the acceptance and flux measurements, we obtain from the largest fluctuation[11] in each sample the upper limits (90% confidence) given in Table V. Individual two-body final states can also be used in the same manner and the results are also contained in this table.

TABLE V. Upper limits on formation of a narrow state in $\bar{p}p$ annihilations.

Final state	Upper limit $B\int\sigma dE$ (μb MeV)
Λ+neutrals	7.9
$\Lambda(\bar{\Lambda}+\bar{\Sigma}^0)$	3.5
$\Lambda\bar{\Lambda}(1520)$	4.9
K^0+ neutrals	25.0
$K^0K^{*0}(890)$	1.6

V. HYPERCHARGE-EXCHANGE REACTIONS

One simple explanation for the two distinct slopes in the differential cross section for $\bar{\Lambda}\Lambda$ and $\bar{\Lambda}\Sigma^0$ is the existence of at least two exchange mechanisms which transfer hypercharge. Thus a comparison of these data with similar data in other hypercharge-exchange reactions such as $\pi^- p \to K^0\Lambda$, as by Abramovich *et al.*,[12] is instructive. Their fit to the differential cross section for this reaction with the parametrization of Eq. (8) is given in Table IV. Another comparison is obtained from the polarization of the hyperon in this reaction with that of the $\bar{\Lambda}$ in the $\bar{\Lambda}\Lambda$ and $\bar{\Lambda}\Sigma^0$ states. In all cases the data show substantial agreement.

The only detailed models of intermediate-energy reactions which predict both the differential cross section and polarization are based on Regge phenomenology. One problem in the use of these models is that for reactions which require more than one exchange process, there is no universally accepted description of the secondary exchange. One hypercharge-exchange model which has been proposed by several authors[2,3] assumes exchange-degenerate $K^*(890)$ and $K^{**}(1420)$ exchange plus an absorptive cut term. The models differ both in the description of the absorptive term and in the parameters which are considered determined by other data. We have applied the model proposed by Plaut[2] to the $\bar{\Lambda}\Lambda$ differential cross sections measured above. The parameters are β_{+-} and β_{++}, the helicity-flip and nonflip couplings at the $K^*p\Lambda$ vertex at $t=0$, E_R, the exponential energy dependence of the Regge residue, and λ_0, the amplitude of the absorption correction in the nonflip amplitude. The other parameters are as specified by Plaut. A similar fit was performed for the $\bar{\Lambda}\Sigma^0$ final state, where β_{++} and β_{+-} are now just fitted parameters related to the Regge residues through factorization. The values which result from the fit are given in Table IV for both the $\bar{\Lambda}\Lambda$ and $\bar{\Lambda}\Sigma^0$ final states, and are displayed in Figs. 5(a) and 5(b). For both reactions the model provides an accurate description of the data, employing, however, as many parameters as the simple exponential functions also given in Table IV. Using these parameters we have also calculated the momentum-transfer dependence of the polarization which is shown in Figs. 5(c) and 5(d). Although the agreement with the data is at best qualitative, the polarization does cross, or become zero, in the t' region predicted by the model.

Our determination of the differential cross section for the final state Λ(forward) + $(\bar{\Lambda},\bar{\Sigma}^0)$ is to date the most statistically significant measurement of

an inelastic process which is forbidden by normal exchange, since only the "exotic" multiplets have $B=2$, $S=-1$ members.

The only reaction requiring a similar u-channel exchange, and for which the differential cross section has been measured, is backward antiproton elastic scattering. The shape near $u'=0$ can be described by $d\sigma/du'=e^{bu'}$, and is rising [$b\sim -1.0$ (GeV/c)$^{-2}$] at 2.84 GeV/c (Ref. 13) incident momentum but may be falling [$b\sim 4.0 \pm 2.0$ (GeV/c)$^{-2}$] at 5.0 GeV/c.[14]

We cannot separate the role of the s-, t-, and u-channel amplitudes in this region. However, the lack of a rise in the differential cross section in the backward direction for our data would tend to exclude an exotic exchange process or a u-channel process involving double baryon exchange. The contribution of the s-channel amplitude cannot be evaluated; however, in Sec. IV we have shown that there are no narrow s-channel states in this energy region.

Thus backward elastic scattering observed by other experiments near our energy appears to be dominated by a continuation of the t-channel amplitude out to $t_{\max}$. For our reaction as well, the smooth monotonic decrease out to $t_{\max}$ also suggests that this is a reasonable interpretation. Extrapolation of the two-body forward $\Lambda^0 d\sigma/du'$ to $-u'=1.67$ (GeV/c)^2 ($\cos\theta^*=0$) yields 2.3 ± 0.5 μb/(GeV/c)^2 compared to the value of the $\bar{\Lambda}^0\Lambda$ plus $\bar{\Lambda}^0\Sigma^0 d\sigma/dt'$, extrapolated to the same point using Eq. (8), of 2.6 ± 0.4 μb/(GeV/c)^2.

VI. SUMMARY AND CONCLUSIONS

We have performed the highest-statistics measurement of the reaction

$$\bar{p}p \to V^0 + \text{neutrals}$$

to date. The two-body final states $\bar{\Lambda}\Lambda$ and $\bar{\Lambda}\Sigma^0$ were extracted from the missing mass to obtain the differential cross section and polarization. For both reactions, $d\sigma/dt'$ shows a forward slope of ≈ 8 and an abrupt change to a slope of ≈ 2 at $-t'\approx 0.35$ (GeV/c)^2. At low $-t'$, the polarization has a positive slope and turns over and either becomes zero or crosses zero near $-t'=0.25$. The differential cross-section results are compatible with some proposed Regge models.[2]

We have also made the first measurement of $d\sigma/du'$ for $\bar{p}p \to \Lambda + (\bar{\Lambda}, \bar{\Sigma}^0)$. The slope strongly suggests that exotic particles in the u channel are not playing an important role in these processes.

Finally, we have set limits on the coupling of a narrow state such as η_c to several two-body final states in the mass range near 2751 MeV/c^2.

ACKNOWLEDGMENTS

This work was supported by the U. S. Department of Energy and the National Science Foundation. We wish to acknowledge the cooperation of the physicists and technicians of the Lindenbaum-Ozaki Group at BNL without whose perseverance the MPS would never have been built. Several other members of our groups have contributed at various stages of this experiment; we would like to express our thanks to Professor J. Bensinger and Professor N. Horowitz, as well as to S. Gottesman, R. Aidun, H. Kooy, and P. Gauthier. We also wish to thank our technicians, Mabel Love, Ida Mongeon, and Betty Osborne, for their dedication.

[1] E. Platner *et al.*, in *Proceedings of the 1973 International Conference on Instrumentation for High Energy Physics, Frascati, Italy, 1973,* edited by S. Stipcich (Laboratori Nazionali del Comitato Nazionale per l'Energia Nucleare, Servizio Documentazione, Frascati, 1973), p. 672.

[2] G. Plaut, Nucl. Phys. B35, 221 (1971).

[3] B. Sadoulet, Nucl. Phys. B53, 135 (1973).

[4] H. W. Atherton *et al.*, Nucl. Phys. B69, 1 (1974). References to earlier publications may be found in this paper.

[5] T. Appelquist and H. D. Politzer, Phys. Rev. Lett. 34, 43 (1975); M. Gaillard *et al.*, Rev. Mod. Phys. 47, 277 (1975); T. Appelquist *et al.*, Phys. Rev. Lett. 34, 365 (1975); J. Mathur *et al.*, Phys. Rev. D 11, 2572 (1975); A. De Rújula *et al.*, *ibid.* 12, 147 (1975); H. Schnitzer, *ibid.* 13, 74 (1976).

[6] J. R. Bensinger *et al.*, Nucl. Phys. B119, 77 (1977).

[7] B. H. Wiik, in *Proceedings of the 1975 International Symposium on Lepton and Photon Interactions at High Energies, Stanford, California,* edited by W. T. Kirk (SLAC, Stanford, 1976), p. 69.

[8] R. Schwitters, in *Particles and Fields '76,* Proceedings of the Annual Meeting of the Division of Particles and Fields of the APS, edited by H. Gordon and R. Peierls (BNL, Upton, New York, 1977), p. A33.

[9] W. Braunschweig *et al.*, Phys. Lett. 67B, 243 (1977).

[10] C. Quigg and J. Rosner, Phys. Rev. D 16, 1497 (1977).

[11] The upper limit is calculated assuming a background given by the center-of-mass energy spectrum for $\bar{\Lambda}$ events. In the interval containing the largest number of events above background, a resonance is hypothesized to exist with a signal given by the observed number of events minus the background. The 90% confidence level is obtained by assuming that this signal results from a 1.65-standard-deviation fluctuation downward from a larger number of true events.

[12] M. Abramovich *et al.*, Nucl. Phys. B27, 477 (1971).

[13] H. Crawley *et al.*, Phys. Rev. D 8, 2012 (1973).

[14] V. Chabaud *et al.*, Phys. Lett. 38B, 449 (1972).